NONLINEARITY AND CHAOS IN ENGINEERING DYNAMICS

Edited by

J. M. T. Thompson
S. R. Bishop

Centre for Nonlinear Dynamics,
University College London, UK

JOHN WILEY & SONS
Chichester · New York · Brisbane · Toronto · Singapore

Baffins Lane, Chichester,
West Sussex PO19 1UD, England
National Chichester (0243) 779777
International (+44) 243 779777

Other Wiley Editorial Offices

John Wiley & Sons, Inc., 605 Third Avenue,
New York, NY 10158-0012, USA

Jacaranda Wiley Ltd, 33 Park Road, Milton,
Queensland 4064, Australia

John Wiley & Sons (Canada) Ltd, 22 Worcester Road,
Rexdale, Ontario M9W 1L1, Canada

John Wiley & Sons (SEA) Pte Ltd, 37 Jalan Pemimpin #05-04,
Block B, Union Industrial Building, Singapore 2057

Library of Congress Cataloging-in-Publication Data

IUTAM Symposium (1993:University College London)
Nonlinearity and chaos in engineering dynamics: IUTAM Symposium,
UCL, July 1993/edited by J. M. T. Thompson, S. R. Bishop.
p. cm.
Includes bibliographical references and index.
ISBN 0-471-94458-0
1. Dynamics—Congresses. 2. Nonlinear theories—Congresses.
3. Chaotic behavior in systems—Congresses. I. Thompson, J. M. T.
II. Bishop, S. R. III. Title.
TA352.I98 1993
620.1'04—dc20

British Library Cataloguing in Publication Data

A catalogue record for this book is available from the British Library
ISBN 0 471 94458 0

Typeset 10½/12pt Palatino by Thomson Press (India) Ltd, New Delhi
Printed and bound in Great Britain by Bookcraft (Bath) Ltd.

15 REGULAR AND CHAOTIC ROTATIONS OF A SATELLITE IN SUNLIGHT FLUX

V. V. Beletsky and E. L. Starostin

Three-dimensional motion of a symmetrical satellite about its centre of mass under the solar radiation torques is considered. The satellite has an axially symmetrical solar stabilizer and a set of reflecting paddles arranged like a windmill. The equations in evolutionary variables are studied. The phase-space structure is investigated. By means of numerical computation of Poincaré maps, the phase trajectories are built. The regular (resonant and quasi-periodic), semi-regular (intermittent) and chaotic trajectories are distinguished. The evolution of phase portraits with change of parameters has been traced.

15.1 INTRODUCTION

Small Space Lab (SSL) is the basic spacecraft for the REGATTA missions. One-axis sun-pointing attitude orientation and stabilization, as well as spin-rate control are planned using solar-radiation pressure. For this purpose, the spacecraft is equipped with an axially symmetric solar stabilizer made from thin films and eight mirror-like solar paddles mounted symmetrically like windmill vanes (Figure 15.1).

SSL spacecrafts are intended for a variety of scientific experiments related to such fields as astrometry, plasma physics and planetary exploration.

The centre of mass of the spacecraft is assumed to move in a circular heliocentric orbit. We study the three-dimensional motion of a symmetric statellite about its centre of mass under the solar-radiation torques. No control of the motion is considered in this chapter.

15.2 MODEL AND EQUATIONS

For such a satellite, we can use the following model of radiation-pressure torque (Beletsky 1966; Beletsky and Starostin 1991):

Nonlinearity and Chaos in Engineering Dynamics
Edited by J. M. T. Thompson and S. R. Bishop.

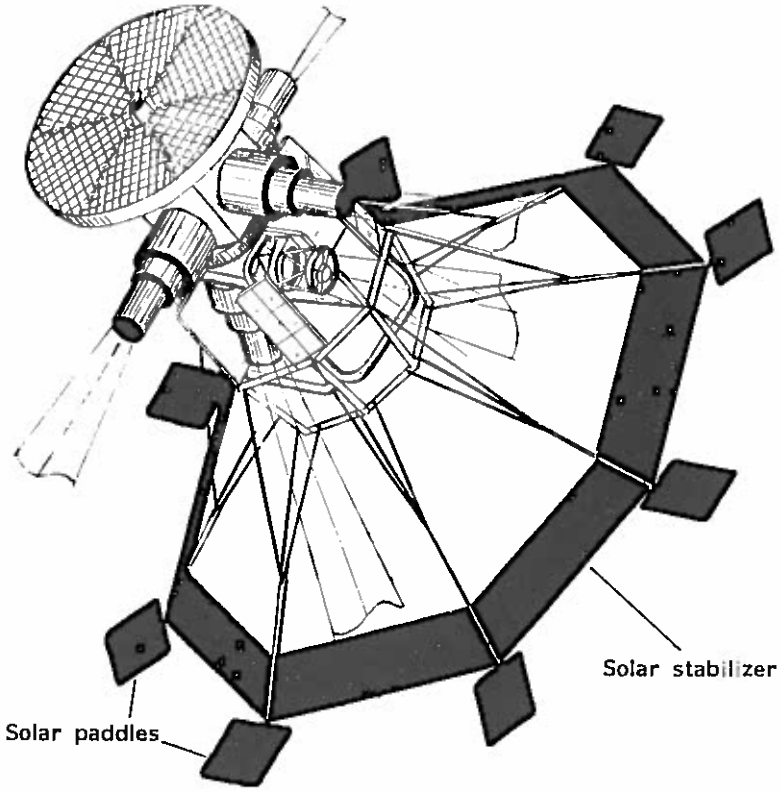

Figure 15.1 General view of Small Space Lab.

$$\boldsymbol{M} = a_s \boldsymbol{e}_r \times \boldsymbol{e}_{z'} + f_s(-a_1\gamma, -a_1\gamma', a_0\gamma'')^{\mathrm{T}}, \tag{1}$$

$$a_s = p_s(R_0/R)^2(a_{s0} + a_{s1}\cos\varepsilon_s + a_{s2}\cos^2\varepsilon_s + \ldots),$$

$$a_{si} = \text{const}, \quad a_{si} \geqslant 0, \quad i = 0, 1, \ldots,$$

$$f_s = 2aS_p n_0 n_1 p_s (R_0/R)^2.$$

Here, R_0 and R are the fixed and the current orbital radius, respectively; $\boldsymbol{e}_r$ is the unit vector in the direction of the orbital radius vector $\boldsymbol{R}$; $\boldsymbol{e}_{z'}$ is the unit vector along the satellite's axis of symmetry z'; $\varepsilon_s = \angle(\boldsymbol{e}_r, \boldsymbol{e}_{z'})$; a is the distance between the centre of a paddle and the axis of symmetry; n_0 is the cosine of the angle between the normal to a paddle and the axis of symmetry; $n_1 = \sqrt{1 - n_0^2}$; S_p is the total area of the paddles; p_s is the solar-pressure constant (for the Earth orbit $R_0 = 1.496 \times 10^{11}$ m and $p_s = 4.64 \times 10^{-6}$ Pa); a_0 and a_1 are the positive coefficients of the model torque; γ, γ' and γ'' are the projections of $\boldsymbol{e}_r$ on the principal axes of inertia of the satellite.

First, we put $a_{s0} = bS > 0$, $a_{sj} = 0$, $j = 1, 2, \ldots$, where b is the distance between the centre of pressure and the centre of mass of the satellite, both the centres lying on the axis of symmetry; S is the satellite's characteristic section area.

The torque of equation (1) consists of the 'conservative' part (the cross-product) and the 'propelling torque', projections of which are written onto principal axes of inertia of the satellite.

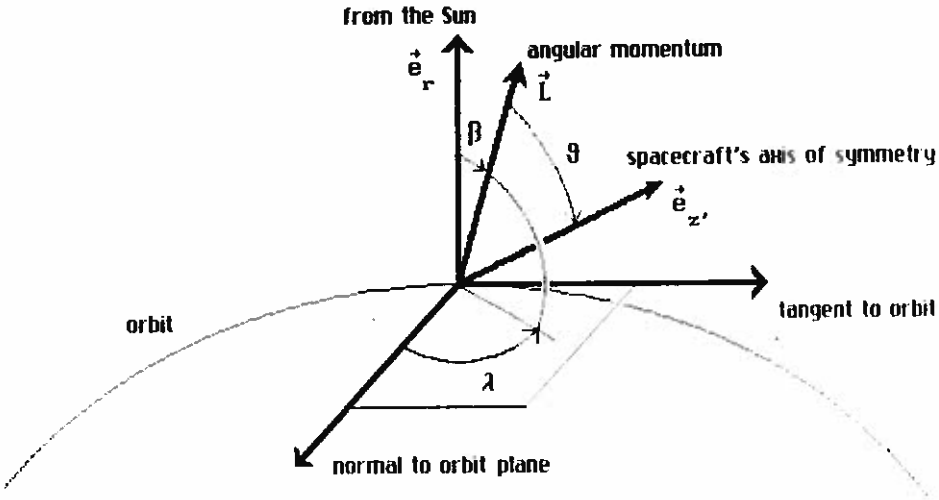

Figure 15.2 Angles ϑ, β and λ.

We employ the first-order approximation equations of motion in evolutionary variables:

$$\begin{aligned}
\frac{dl}{d\tau} &= f(\cos^2\vartheta - \alpha)\cos\beta,\\
\frac{d\vartheta}{d\tau} &= -\frac{f}{l}\sin\vartheta\cos\vartheta\cos\beta,\\
\frac{d\beta}{d\tau} &= -\varepsilon\sin\lambda + \frac{f}{l}(\alpha - \tfrac{1}{2}\sin^2\vartheta)\sin\beta,\\
\frac{d\lambda}{d\tau} &= -\varepsilon\cot\beta\cos\lambda + \frac{1}{l}\cos\vartheta,
\end{aligned} \tag{2}$$

$$f = (a_0 + a_1)\frac{2aS_p n_0 n_1}{bS}, \quad \alpha = \frac{a_1}{a_0 + a_1}, \quad \varepsilon = \frac{L_0\sqrt{\mu R}}{bSp_s R_0^2},$$

where $l = L/L_0$ is the dimensionless module of the angular momentum vector $\boldsymbol{L}$ of the spacecraft, L_0 is a fixed value of the angular momentum module; $\vartheta = \angle(\boldsymbol{L}, \boldsymbol{e}_{z'})$; $\beta = \angle(\boldsymbol{e}_r, \boldsymbol{L})$; λ is the angle between the normal to the orbit plane and the projection of the vector $\boldsymbol{L}$ on the plane orthogonal to $\boldsymbol{e}_r$ (Figure 15.2); τ is the dimensionless time, $\varepsilon\tau = \nu$, ν is the true anomaly of the orbit; α is the design variable; μ is the gravity constant of the Sun.

15.3 ANALYSIS OF EQUATIONS

In equations (2) the term $(1/l)\cos\vartheta$ describes a conservative effect, the terms $\sim f$ describe an effect of 'propelling' due to the screw-symmetrical paddles, and the terms with λ are due to the orbital motion.

The conservative effect reduces to precession of the angular momentum vector (at small ε approximately around the direction to the Sun with rate $d\lambda/d\tau \sim (1/l_0)\cos\vartheta_0$). The propelling effect causes profound modulations of the angular momentum vector orientation with respect to this direction (i.e. the modulations of the angle β); at the same time, the variables l and ϑ exhibit similar modulations (Figures 15.3 and 15.4). The combination

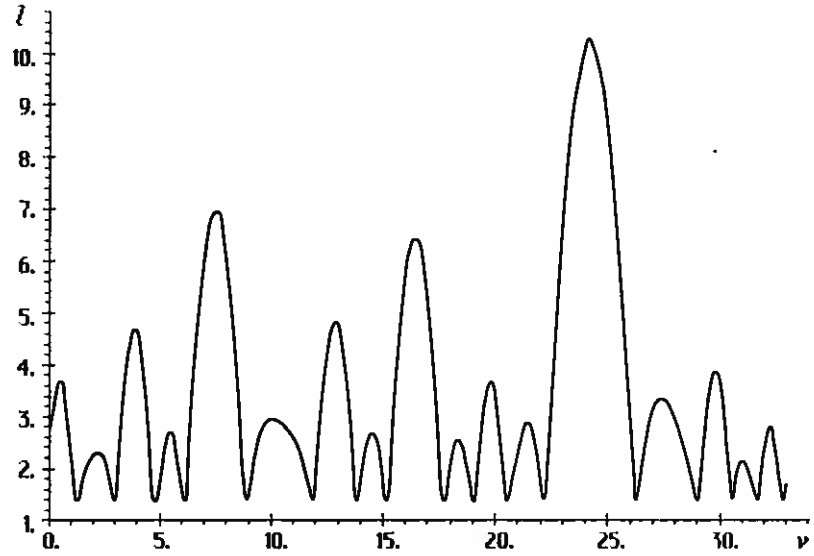

Figure 15.3 Angular momentum module l versus true anomaly ν. $f = 0.15$, $\varepsilon = 0.01$; $\alpha = 0.3$, $\lambda_0 = 0.0$, $l_0 = 2.38$.

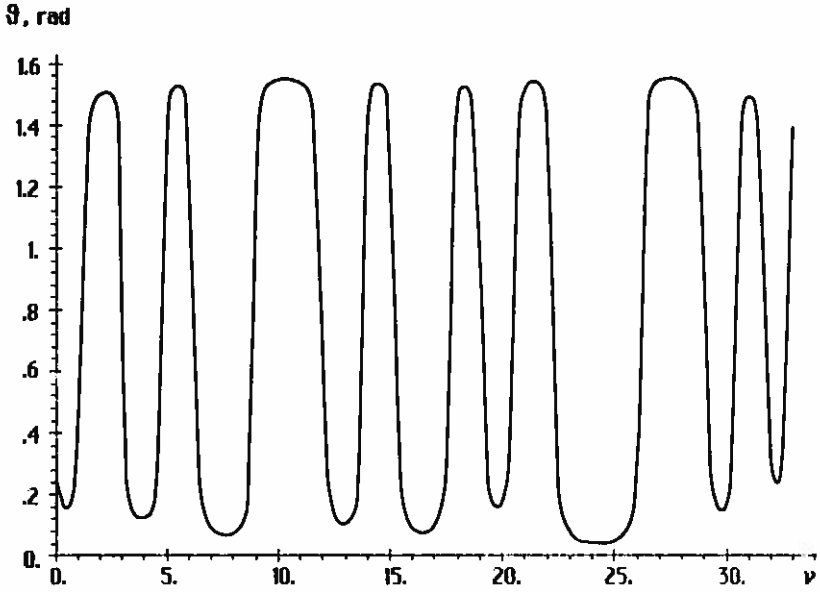

Figure 15.4 Angle ϑ versus true anomaly ν, corresponding the previous figure.

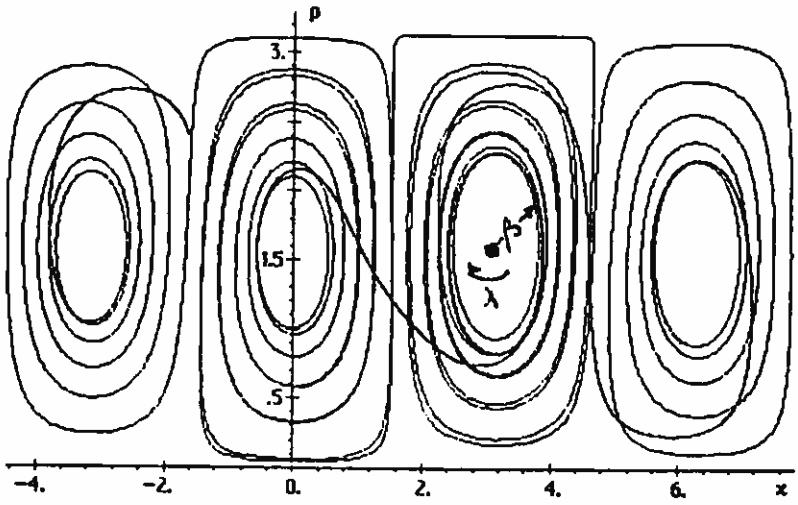

Fifure 15.5

of these two effects results in the peculiar picture of 'pulsing' precession of the vector $\boldsymbol{L}$ around the radius vector direction (Figure 15.5). The most interesting fact is the abrupt jumps from the motion in the vicinity of the direction *to* the Sun into the motion in the neighbourhood of the direction *from* the Sun. Such jumps are often difficult to predict. This stochasticity is inherent in the dynamical system (2) and it can be represented clearly in the appropriate phase space.

The primitive integral gives:

$$l \cot^{\alpha} \vartheta \sin \vartheta = C. \tag{3}$$

This enables the system order to be reduced to three, by elimination of the variable l, and to two by employing λ as a new independent variable. The second-order system obtained is non-autonomous and periodic in λ. In the phase space (ϑ, β), with C fixed, the motion may be generally described by the complex regular and chaotic trajectories, revealed by the numerical implementation of the Poincaré mapping. The plane (ϑ, β) is chosen as a surface of section and λ-mapping over 2π is studied.

For some values of the parameters, the set of trajectories may comprise only regular ones. Such cases are said to be completely integrable. An autonomous system of the third order is completely integrable if it admits of only one primitive integral.

Let us fix the parameters α and C. Then system (2) has two free parameters, f and ε. Consider behaviour of system (2) for extreme values of f and ε, remembering the following from integral (3).

1. If $\varepsilon^{-1} = 0$, another integral exists:

$$\sin^2 \beta \cos^2 \lambda \cos \vartheta \tan^{2\alpha} \vartheta = C_1.$$

and system (2) is completely integrable. There are no chaotic trajectories.

2. If $\varepsilon = 0$, then for $\varepsilon \ll 1$, it can be seen from the last of equations (2) that λ is the fast variable and equations (2) can be averaged with respect to λ, the averaged system (2)

having the primitive integral

$$\sin^2\beta\cos\vartheta\tan^{2\alpha}\vartheta = \bar{C}_1. \tag{4}$$

and being completely integrable. The initial (non-averaged) system (2) is close to the completely integrable system; the absence of chaos (or weak chaos) can be predicted.

3. When $f = 0$, the system (2) has first integrals

$$l = l_0, \quad \vartheta = \vartheta_0, \quad \varepsilon\sin\beta\cos\lambda + \frac{1}{l_0}\cos\vartheta_0\cos\beta = \Phi_0, \tag{5}$$

and all its trajectories are regular.

4. When $f^{-1} = 0$, the term $\varepsilon\sin\lambda$ in the third of equations (2) may be neglected. Integral (4) exists. The system is close to a completely integrable one.

It is worth noting that the consideration of items 2 and 4 may be expressed in mathematical terms.

When considering the question of whether the angle λ is a monotonic function of time or not it is noted that this condition does not always hold; i.e. the phase trajectories may be tangent to the chosen section plane (ϑ, β). Hence, when constructing the Poincaré map, the possibility should be taken into consideration that a trajectory, having come out of a point of the section $\lambda = 0$, may return and intersect the same plane once more, having not reached the section $\lambda = 2\pi$ (or $\lambda = -2\pi$).

To examine the mechanism of this in more detail we consider the system (2) when $f = 0$ once again by examining the third primitive integral (5) $\Phi(l_0, \vartheta_0; \beta, \lambda)$. Locating the critical points of the function Φ treated as a function of two variables, angles β and λ, the first partial derivatives can be calculated as:

$$\frac{\partial\Phi}{\partial\beta} = \varepsilon\cos\beta\cos\lambda - \frac{1}{l_0}\cos\vartheta_0\sin\beta,$$

$$\frac{\partial\Phi}{\partial\lambda} = -\varepsilon\sin\beta\sin\lambda.$$

Both the derivatives become zero in two cases when:

$$\begin{aligned} &1)\ \beta = \pi i, && i = 0, \pm 1, \pm 2, \ldots; \\ &\quad \lambda = \pi/2 + \pi k, && k = 0, \pm 1, \pm 2, \ldots; \end{aligned} \tag{6}$$

$$\begin{aligned} &2)\ \beta = \pm\beta^* + \pi m, && m = 0, \pm 1, \pm 2, \ldots; \\ &\quad \lambda = \pi n, && n = 0, \pm 1, \pm 2, \ldots; \end{aligned} \tag{7}$$

where β^* is a root of the equation $(d\lambda/d\tau)|_{\lambda=0} = 0$.

If one calculates the second partial derivatives Φ_{ij} and finds $\det\Phi_{ij}$, then it will turn out that in case (6) $\det\Phi_{ij} = -1$ and it can be shown that in case (7) $\det\Phi_{ij} > 0$. Therefore, case (6) corresponds to unstable critical points of the function Φ (saddles) and case (7) to stable centres. The trajectories that originate from the section $\lambda = 0$ in the vicinity of the stable point, never reach the neighbouring section $\lambda = 2\pi$ (-2π) (Figure 15.6).

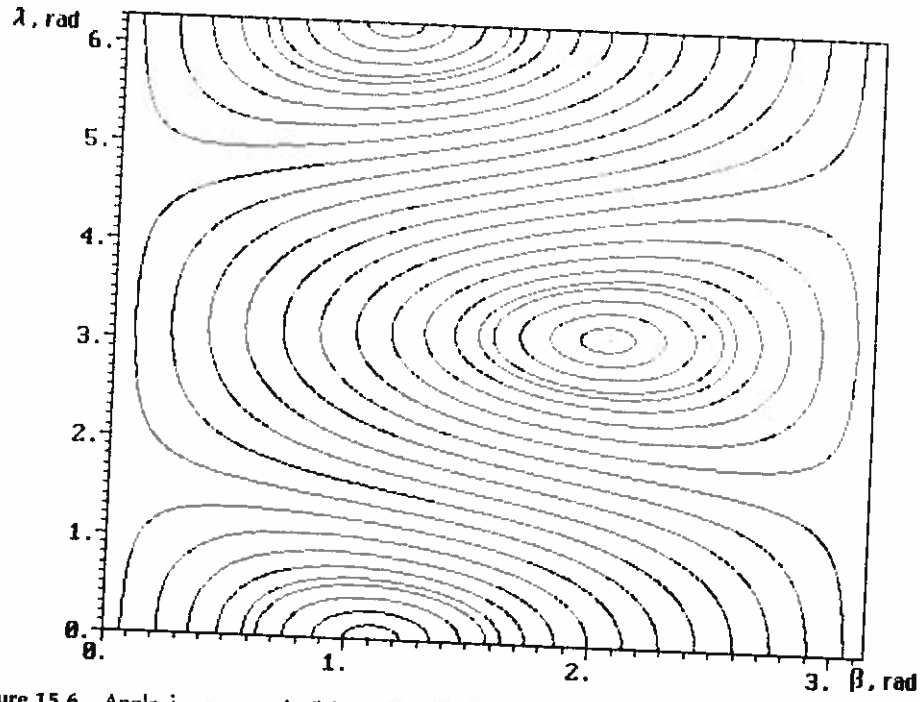

Figure 15.6 Angle λ versus angle β for various initial values of angle β. $f = 0$, $\varepsilon = 1$, $\vartheta = \pi/4$, $C = 1$.

A similar picture takes place for $f \neq 0$. The only difference is that, in the general case, there are no separatrices between stable and unstable points and trajectories may go from the vicinity of the stable point to the neighbourhood of the unstable one and vice versa. When computing the Poincaré map of the section $\lambda = 0$, a trajectory of system (2) is traced until it intersects any of the sections $\lambda = 0, \pm 2\pi$. By numerical integration when a trajectory is about to intersect the section plane $\lambda = 0 \pmod{2\pi}$, system (2) is substituted by an equivalent system with independent variable λ. This is done in order to find the intersection point with precision.

At $f = 0$ the stable critical points (7) constitute a curve in the (ϑ, β) plane – the derivative $d\lambda/d\tau$ vanishes on this curve. Similar curves exist in the general case, too, marked by S–S in Figures 15.9–11.

15.4 POINCARÉ MAPPING

A global analysis of the phase space was carried out and the evolution of surfaces of section were traced out with a variation of the parameters. The results obtained make it possible to specify design conditions for SSL. For astrometrical studies, the predictability of the spacecraft motion is critical, therefore the regions of chaotic motions must be avoided. On the other hand, there are scientific experiments that require the whole celestial sphere to be scanned, and in those cases chaotic rotation may be very desirable.

The following values were taken: $\alpha = 0.3$ (for all the following pictures except Figure 15.12), and $C = 1.0$.

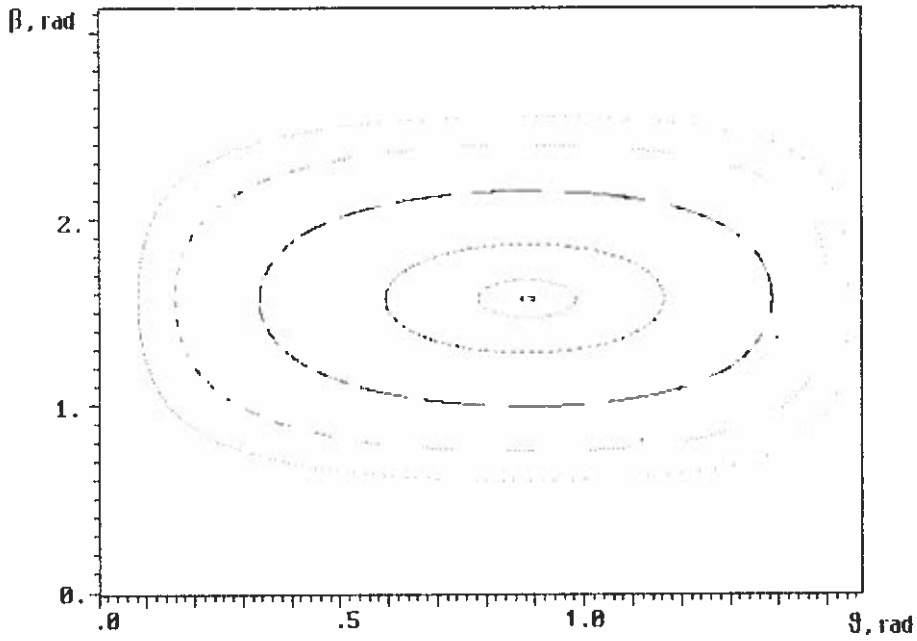

Figure 15.7 Surface of section for $f = 0.15$, $\varepsilon = 0.0$.

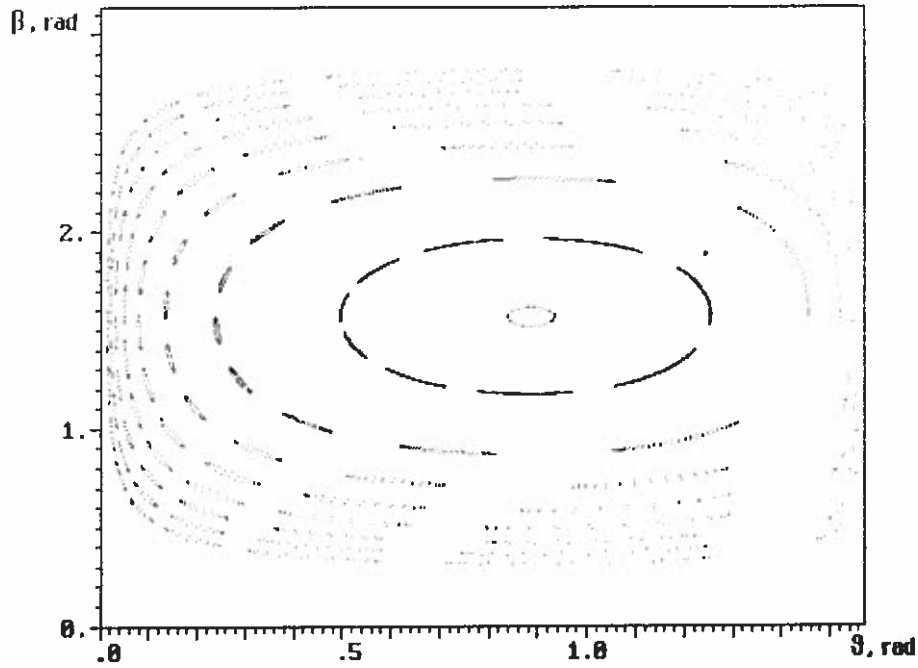

Figure 15.8 Surface of section for $f = 0.15$, $\varepsilon = 4.42 \times 10^{-5}$.

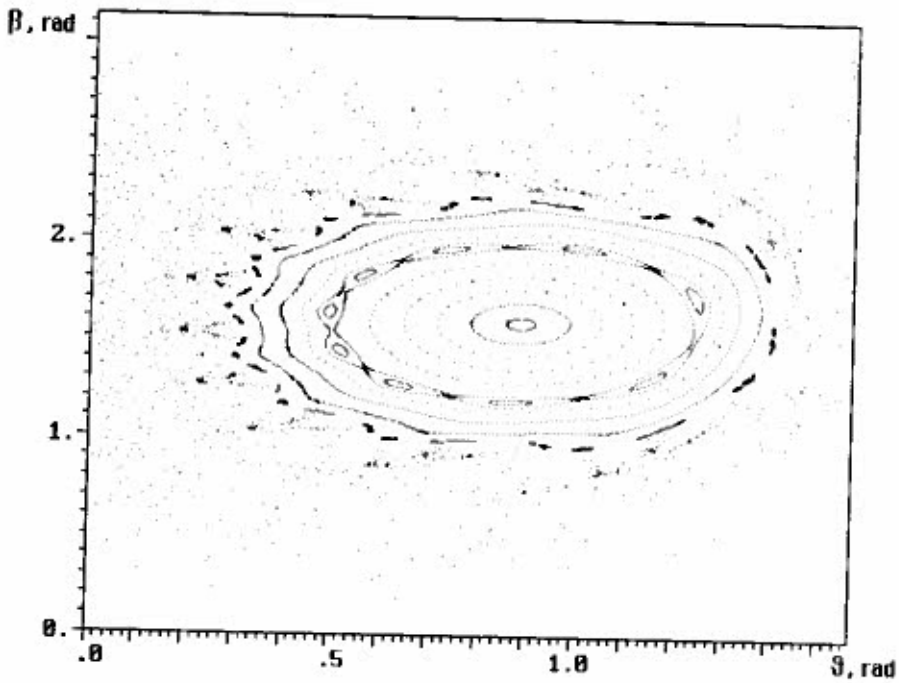

Figure 15.9 Surface of section for $f = 0.15$, $\varepsilon = 0.01$.

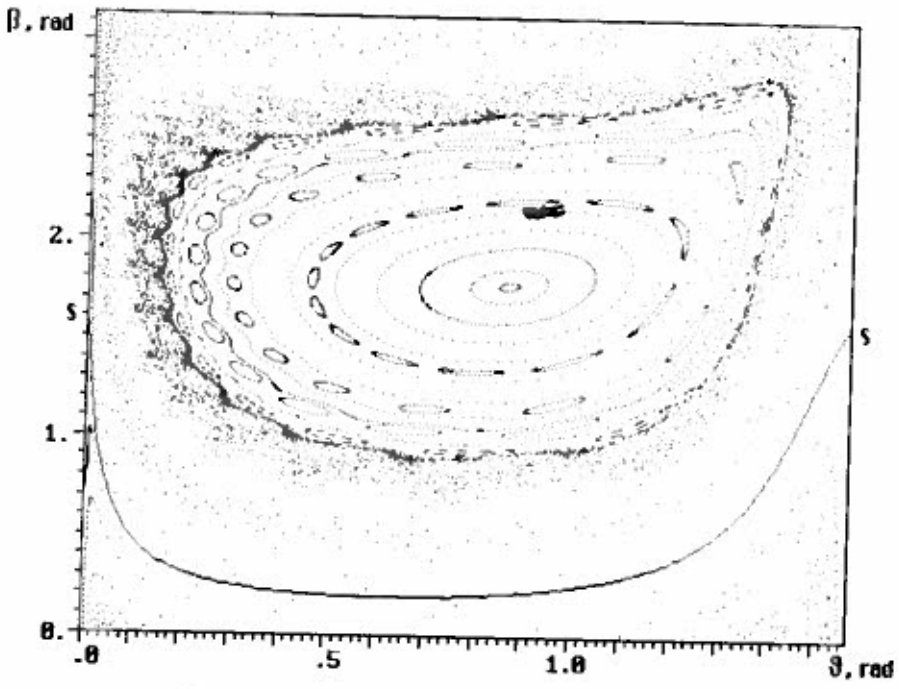

Figure 15.10 Surface of section for $f = 0.105$, $\varepsilon = 0.1$.

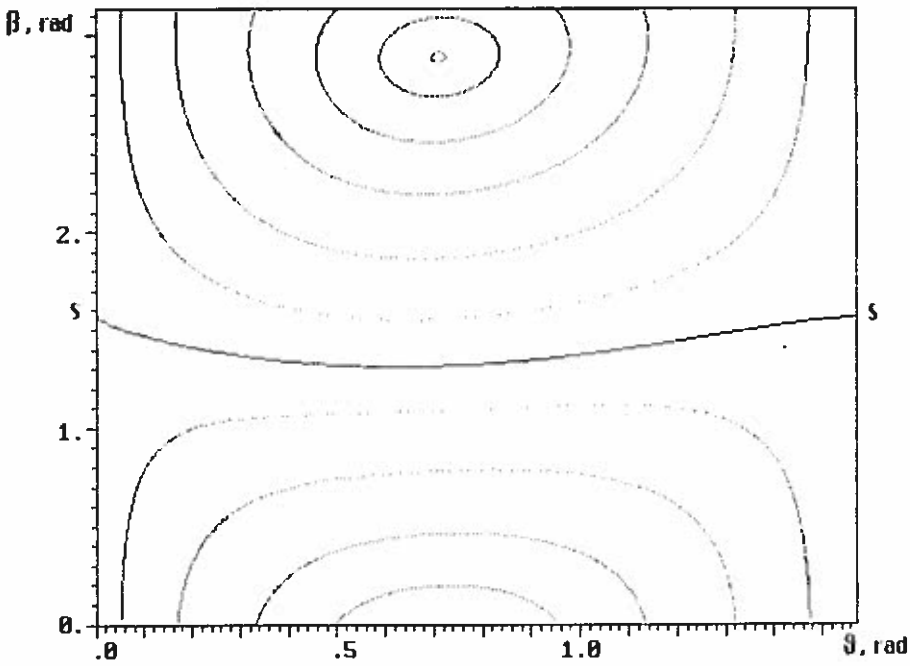

Figure 15.11 Surface of section for $f = 1.05$, $\varepsilon = 2.0$.

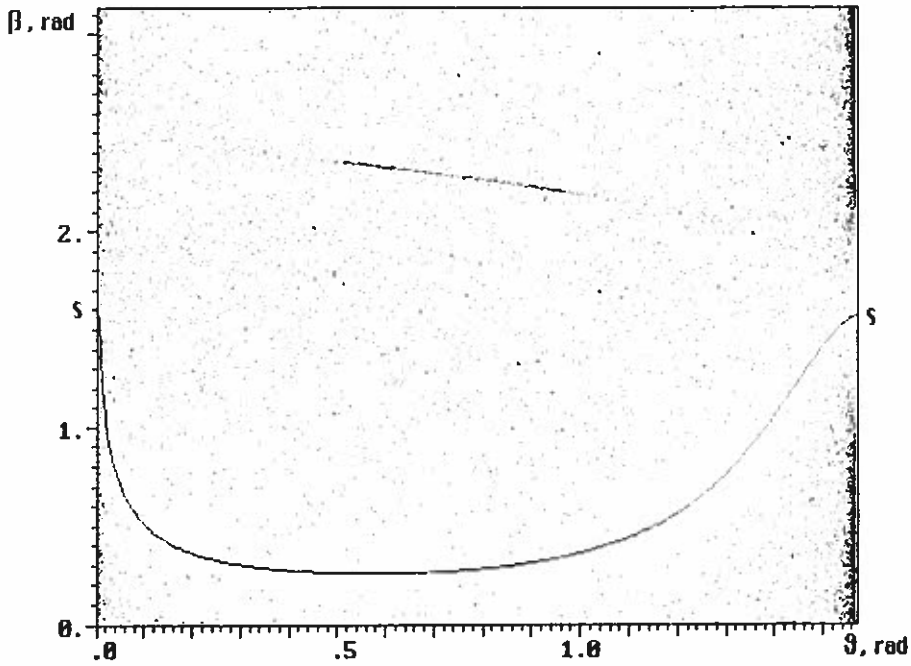

Figure 15.12 Surface of section for $f = 1.5$, $\varepsilon = 0.14$, $\alpha = 0.4225$.

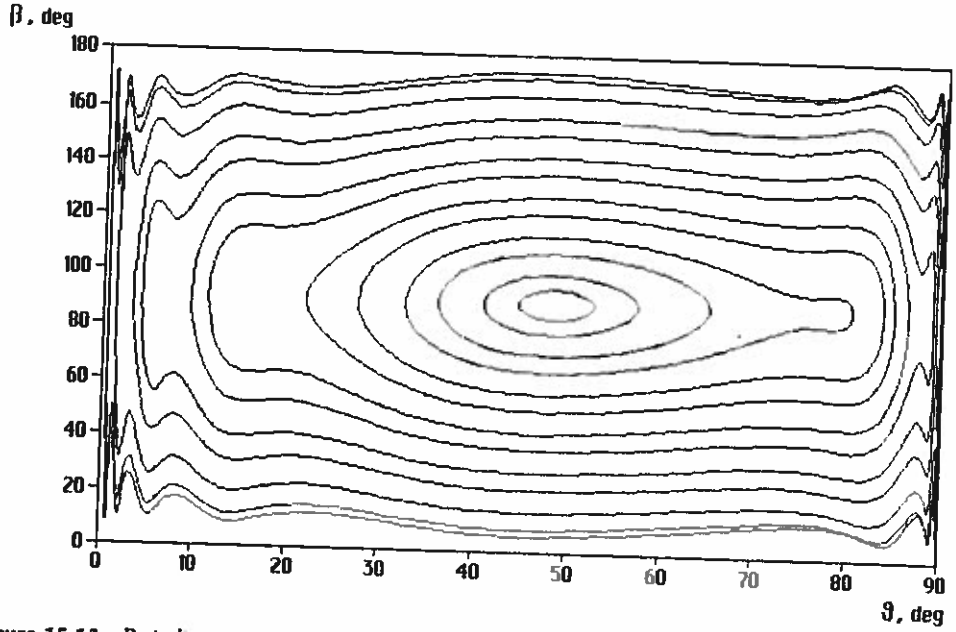

Figure 15.13 Periodic motions in the case $\alpha_{s1} > 0$, $\alpha_{sj} = 0$, $j = 0, 2, \ldots$, $f = 0.15$, $\varepsilon = 0.01$, $\alpha = 0.3$, $\lambda_0 = 0.0$, $l_0 = 2.38$.

Figure 15.7 is displayed for $f = 0.15$, $\varepsilon = 0.0$. There is no stochasticity detected. In Figure 15.8 ($f = 0.15$, $\varepsilon = 4.42 \times 10^{-5}$) one can see some curves splitting and chains of islands appearing. The stochasticity layers are thin and separated.

It should be noted that boundaries $\vartheta = 0$, $\vartheta = \pi/2$, $\beta = 0$, $\beta = \pi$ play the role of separatrices of the family (4); therefore, stochasticity should be expected near these boundaries first, and the 'centre' of the region is less affected by stochasticity. Figure 15.9 confirms this ($f = 0.15$, $\varepsilon = 0.01$).

Figure 15.10 ($f = 0.105$, $\varepsilon = 0.1$) exhibits development of the chaos. One can observe regularization of chaotic trajectories near the curve S–S. The nearer to the curve S–S the trajectory approaches the slower the point moves along it. Therefore, these trajectories exhibit intermittent behaviour.

Figure 15.11 ($f = 1.05$, $\varepsilon = 2.0$) reveals that the motion becomes almost completely regular. On the other hand, strong stochasticity takes place for $f = 1.5$, $\varepsilon = 0.14$ and $\alpha = 0.4225$ (Figure 15.12). Only one trajectory is presented in this figure. As α increases, global stochasticity occurs.

Let us now revert to the radiation-pressure torque expression (1). Put $a_{s1} > 0$, $a_{sj} = 0$, $j = 0, 2, \ldots$ (Beletsky *et al.* 1992). Then the last of equations (2) is found to be

$$\frac{d\lambda}{d\tau} = -\varepsilon \cot\beta \cos\lambda + \frac{1}{l}\left(\tfrac{3}{2}\sin^2\vartheta - 1\right)\cos\beta.$$

Numerical experiments reveal that in this case all trajectories turned out to be periodic (Figure 15.13). No stochasticity was found at any set of parameters. The motion of the satellite is easy to predict.

REFERENCES

Beletsky, V. V. (1965) *Motion of an Artificial Satellite about its Center of Mass*, Jerusalem, Israel Program for Scientific Translations.

Beletsky, V. V. and Starostin, E. L. (1991) Regular and chaotic rotions of the satellite in sunlight flux, Keldysh Inst. of Appl. Math., preprint No 68 [in Russian].

Beletsky, V. V., Prokofyeva, E. V. and Starostin, E. L. (1992) Spacecraft rotational dyanmics in light flux, Keldysh Inst. of Appl. Math., preprint No 47 [in Russian].

V. V. Beletsky and E. L. Starostin, *M. V. Keldysh Institute of Applied Mathematics, Russian Academy of Sciences, 4 Miusskaya Square, 125047 Moscow, Russia*